10.1098/rspa.2001.0915

THE ROYAL SOCIETY

The slump origin of the 1998 Papua New Guinea Tsunami

By Costas E. Synolakis[1]†, Jean-Pierre Bardet[1], José C. Borrero[1], Hugh L. Davies[2], Emile A. Okal[3], Eli A. Silver[4], Suzanne Sweet[4] and David R. Tappin[5]

[1]*Department of Civil Engineering, University of Southern California, Los Angeles, CA 90089, USA*
[2]*Geology Department, University of Papua New Guinea, University PO, NCD [Port Moresby], Papua New Guinea*
[3]*Department of Geological Sciences, Northwestern University, Evanston, IL 60208, USA*
[4]*Earth Sciences Department, University of California, Santa Cruz, CA 95064, USA*
[5]*British Geological Survey, Keyworth, Nottingham NG12 5GG, UK*

Received 11 June 2001; accepted 3 September 2001; published online 1 February 2002

The origin of the Papua New Guinea tsunami that killed over 2100 people on 17 July 1998 has remained controversial, as dislocation sources based on the parent earthquake fail to model its extreme run-up amplitude. The generation of tsunamis by submarine mass failure had been considered a rare phenomenon which had aroused virtually no attention in terms of tsunami hazard mitigation. We report on recently acquired high-resolution seismic reflection data which yield new images of a large underwater slump, coincident with photographic and bathymetric evidence of the same feature, suspected of having generated the tsunami. T-phase records from an unblocked hydrophone at Wake Island provide new evidence for the timing of the slump. By merging geological data with hydrodynamic modelling, we reproduce the observed tsunami amplitude and timing in a manner consistent with eyewitness accounts. Submarine mass failure is predicted based on fundamental geological and geotechnical information.

Keywords: tsunamis; Papua New Guinea; slumps; hydroacoustics; hydrodynamic simulation

1. Introduction

On 17 July 1998, a tsunami struck the area of Sissano Lagoon, Sandaun Province, Papua New Guinea (PNG), *ca.* 20 min after a nearby magnitude 7 earthquake, which took place at 08.49 GMT (18.49 local time). A 25 km segment of the northwestern PNG coastline, home to at least 10 000 people, was swept clean by ocean waves averaging 10 m in height (figure 1), with over 2100 people killed during the tsunami or shortly afterwards (Davies 1998; Kawata *et al.* 1999). At teleseismic distances, tidal gauges in Japan recorded the tsunami with amplitudes not exceeding 25 cm.

† Co-authors of Synolakis are listed alphabetically.

The singular character of this exceptionally devastating tsunami is underscored by the geographical concentration of the devastation along the shoreline, and by the moderate size of its parent earthquake, for which magnitude estimates are $m_b = 5.9$, $M_s = 7.0$, $M_m = 6.8$ (Okal & Talandier 1989), with a final Harvard moment of only 3.7×10^{26} dyn cm (Dziewonski *et al.* 1999). The energy-moment test of Newman & Okal (1998) yielded $\Theta = -5.50$, indicating that the earthquake does not exhibit the exceptionally slow source behaviour ($\Theta < -6.0$) shown by recent 'tsunami earthquakes', whose tsunamis were disproportionately large given the amplitude of their seismic waves (Kanamori 1972; Newman & Okal 1998; Polet & Kanamori 2000). This evidence, gathered in the few hours following the disaster, immediately suggested a mechanism other than pure seismic dislocation as the source of the tsunami, in the possible form of a giant submarine mass failure, a broad geological term that includes underwater slides and slumps (Schwab *et al.* 1993).

The possibility that major tsunamis could be generated by massive submarine slumps was recognized a century ago by such visionary scholars as Milne (1898) and Montessus de Ballore (1907). Later, Gutenberg (1939) went as far as advocating that slumps should be considered the primary source of major tsunamis, and Ambraseys (1960) interpreted the 1956 Amorgos, Greece, tsunami as being caused by a series of submarine landslides. In more recent years, a variety of studies has supported the scenario of the generation of a major tsunami by a large submarine mass failure, itself induced or triggered by a large earthquake in a coastal area. In addition to the classical documented cases of Grand Banks in 1929 (Hasegawa & Kanamori 1987), Kalapana, Hawaii in 1975 (Eissler & Kanamori 1987), and the ongoing speculation about the great 1946 Aleutian tsunami (Kanamori 1985; Okal 1992; Pelayo & Wiens 1992), careful analyses of run-up patterns along shorelines often reveal a peaked distribution, with very intense and localized maxima, generally attributed to a local submarine mass failure, against the background of a more regular wave amplitude reflecting the coseismic dislocation. This would be the case, in particular, for localities in Prince William Sound during the great 1964 Alaska earthquake (Plafker *et al.* 1969), at Riangkroko during the 1992 Flores, Indonesia event (Imamura *et al.* 1995), and during the recent Izmit, Turkey earthquake (Yalçiner *et al.* 1999). This scenario can also explain minor tsunamis during strike–slip earthquakes on nearby on-land faults, for example, following the 1989 Loma Prieta earthquake (Ma *et al.* 1991). It is clear that the exact timing of failure in this framework is variable, but delays of a few minutes to a few tens of minutes could easily be attributed to the complex nucleation of a failure plane in metastable sediment, or to a mild secondary trigger (aftershock) tipping a precarious balance (Bjerrum 1971; Murty 1979; Turner & Schuster 1996).

Characteristics of tsunamis generated by the two kinds of sources can be compared in very general terms by noticing that the vertical deformation of the sea floor wrought by an underwater mass failure is controlled by a combination of the dimension of the sliding mass and the motion of its centre of mass, both easily reaching hundreds of metres, while a practical bound on sea floor deformation during even the largest earthquakes is usually several metres (Plafker 1965; Kanamori 1970), exceptionally reaching 20–30 m (Plafker & Savage 1970; Kanamori & Cipar 1974). On the other hand, the linear dimension of an underwater landslide will rarely exceed 100 km (although the resulting turbidity current could extend over a greater distance (Piper & Aksu 1987)), while catastrophic earthquakes can feature coherent rupture along close to 1000 km (Kanamori 1970; Kanamori & Anderson 1975). These

order-of-magnitude arguments then predict that sea floor dislocations will result in tsunamis featuring greater wavelengths and longer periods, and in turn, in a potential for transoceanic devastation, whereas those caused by mass failures are more geographically contained, even though they may give rise to higher amplitudes in the local field (Plafker *et al.* 1969; Schwab *et al.* 1993).

In this general framework, the early recognition of the anomalous character of the PNG tsunami motivated a broad international investigation effort, involving in particular several field expeditions. First, an International Tsunami Survey Team (ITST) visited the PNG site two weeks after the disaster, mapped the maximum run-up, and in the absence of local tide gauge measurements, interviewed survivors to constrain the timing of the wave's arrival at various points along the coast. This latter aspect was pursued systematically by Davies (1998).

Several months later, two marine surveys were carried out on joint cruises of the Japan Marine Science and Technology Center (JAMSTEC) and the South Pacific Applied Geoscience Commission (SOPAC), aboard RV *Kairei* and RV *Natsushima*. The main goal of these expeditions was to obtain the detailed bathymetric coverage required for the accurate simulation of the tsunami propagation under various scenarios of generation. In addition, the deployment of a remotely operated vehicle (ROV) revealed the presence of a recent slump at the foot of an amphitheatre structure identified by the bathymetric survey (Tappin *et al.* 1999, 2001). In September 1999, high-resolution seismic reflection profiles were acquired by RV *Maurice Ewing*; in particular a complete seismic section was obtained over the body of the slump (Sweet *et al.* 1999; Sweet 2000), resulting in a full, three-dimensional model of its structure.

In the meantime, a systematic examination of hydroacoustic records at the Wake Island monitoring station (Okal 1999) revealed the highly anomalous source signature of a small aftershock occurring 13 min after the mainshock, which we interpret as the actual mass failure that resulted in the slump detected by the marine surveys, and that generated the local tsunami.

The organization of this paper follows to a large extent the chronology of the investigation presented above, allowing us to progressively build the case for a slump origin to the PNG tsunami. We present in § 2 the basic seismological framework, followed in § 3 by a description of the principal results acquired during the land surveys. Section 4 details the results of the marine surveys, while § 5 presents the hydroacoustic data. The combination of the geometry revealed by the seismic refraction experiment with the timing suggested by the hydroacoustic study then sets the stage for the full modelling of the resulting tsunami in § 6. Our conclusion is that the local tsunami can be adequately modelled by a massive underwater slump involving 4 km^3 of sediments, which was triggered at 09.02 GMT, 13 min after the main seismic event.

2. Seismological aspects

The seismic sequence of the PNG earthquake comprises the main shock at 08.49.13 GMT, followed by a widely felt aftershock, itself composed of two events at respectively 09.09.32 ($m_b = 5.6$) and 09.10.02 ($m_b = 5.9$). In between, two small aftershocks are documented by the National Earthquake Information Center (NEIC) at respectively 09.02.06 ($m_b = 4.4$) and 09.06.03 (no magnitude reported). A mantle

Figure 1. Map of the Sandaun coast of northwestern Papua New Guinea (black rectangle in inset locates main map). Red open circles on coastline identify devastated villages; solid black circles are other, mostly spared, communities. The large stars are epicentres of the mainshock (blue: initial NEIC; green: final NEIC; white: as relocated in this study, with error ellipse (in blue)). The smaller, grey stars are epicentres of the relocated doublet at 09.09 and 09.10 GMT. The line joining them is the extent of the seismic rupture, as inferred from the seismological modelling of Kikuchi *et al.* (1998). The open yellow-red star is the relocated epicentre of the 09.02 seismic event (with error ellipse in red). The yellow disc schematizes the location of the slump identified by the surveys (see figure 3). The triangle at bottom left is the ISC epicentre (with associated error ellipse). The smaller green dots are other aftershocks relocated in this study.

magnitude $M_m = 5.75$ was obtained for the 09.10 aftershock with a slowness parameter $\Theta = -4.80$, indicating that it was not a slow event. Given its size, it would be even more difficult than for the main shock to reconcile the aftershock with the observed tsunami amplitudes.

The epicentre of the main shock was originally located by the NEIC at 2.932° S; 141.797° E, a few kilometres inland (blue star in figure 1). The final NEIC location, published in the monthly PDE bulletin is at 2.961° S, 141.926° E, along the coastline, immediately west of the village of Serai (green star in figure 1). Our own relocation (2.95° S; 141.96° E; white star) is essentially equivalent. Monte Carlo relocations including Gaussian noise with $\sigma_G = 1$ s (Wysession *et al.* 1991) yield an ellipse of semi-major axis 12 km, oriented east–west. It is futile to attempt a greater precision on the epicentre, which is thus constrained to lie on the shoreline or at most a few kilometres offshore, between the village of Serai and the uplifted shoreline, northwest of the Lumber Mill (see figure 1). This epicentral location marks the westernmost extension of the flat, low lying coastal plain in which Sissano Lagoon developed to its present size, following subsidence during a major earthquake in 1907 (Neuhauss 1911). Farther west, the coast morphology evolves into volcanic cliffs, presumably of Palaeogene age.

The NEIC determinations were carried out at a constrained depth of 10 km; our relocation converged on 21 km when the depth was left floating, although depth resolution was poor; these numbers are in general agreement with Kikuchi *et al.*'s (1998) results, suggesting a hypocentral depth of 15 ± 5 km. These authors also investigated in detail the rupture of the mainshock, which they modelled as extending 35 km eastwards of the hypocentre.

The Harvard Centroid Moment Tensor (CMT) location (2.50° S; 142.07° E) is *ca.* 50 km NNE of the preferred epicentre. While hypocentre and centroid are different concepts which are not expected to coincide, they are, in this particular instance, difficult to reconcile in the framework of a propagating fault, which would have to involve a rupture direction nearly perpendicular to that proposed by Kikuchi *et al.* (1998). Furthermore, the preliminary ('QUICK') Harvard Centroid is located at yet another site (2.78° S; 142.57° E), 63 km from the final centroid, casting some doubt on the robustness and eventual accuracy of the centroid locations, which could be strongly affected by such factors as station distribution. We note in particular that the final Harvard solution is obtained exclusively on the basis of mantle waves at a period of 135 s, whose wavelengths are much too large to help resolve the location of the event on a fine scale. For this reason, we regard the Harvard centroid as irrelevant to the discussion of the precise location of the rupture.

As shown by the triangle in figure 1, the final location proposed for the main shock by the International Seismological Center (ISC) is 40 km inland, southwest of Serai, at 3.20° S, 141.67° E: a very puzzling result. We note, however, a large scatter in their residuals at short distances, generally in excess of the reported standard deviation of the residuals ($\sigma = 1.66$ s). We believe that this stems from the ISC's procedure of working with a fixed dataset comprising all reported arrival times, whereas both the NEIC's and our solutions were achieved through an algorithm eliminating stations with high residuals or obviously erroneous data, such as 'minute phases'. In the presence of complexity in regional propagation at short distances, this can substantially affect the eventual solution, even if a very large number of well-fitted readings at teleseismic distances (in the present case more than 200) can

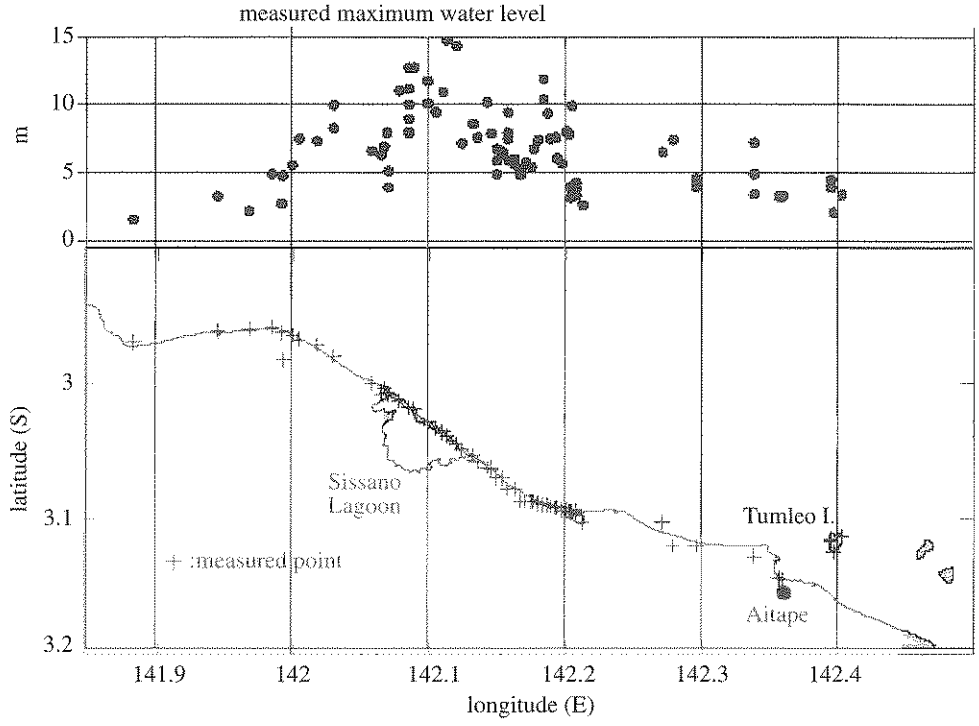

Figure 2. Maximum water heights measured by the ITST. The map at the bottom shows the location of the individual measurements (crosses). The diagram at the top plots the individual heights as a function of longitude along the coast.

artificially reduce the root-mean square residual. As a result, we disregard the ISC epicentre as erroneous, and the reported quality of their solution (as expressed by an error ellipse with a semi-major axis of only 5.7 km) as unrealistic.

Figure 1 also shows our preferred relocations for the 09.02, 09.09 and 09.10 aftershocks. The 09.06 event could not be robustly relocated. All aftershock depths are unresolvable and were constrained at 10 km in the relocations. In Kikuchi *et al.*'s (1998) model, the 09.10 epicentre could represent the eastern end of the rupture area of the mainshock, 30–35 km from its hypocentre.

The focal mechanism of the mainshock (shown by its Harvard centroid moment tensor (Dziewonski *et al.* 1999) in figure 1) can be interpreted as either low-angle oblique subduction of the Caroline segment of the Pacific plate under New Guinea, or high-angle reverse faulting. The former involves a dip of 19° along a fault striking N146° E, the latter a dip of 75° along a plane striking N287° E. When evaluating the performance of the dislocation as the source of the tsunami, the seismologist is faced with the perennial hurdle of choosing between the two focal solutions. As will be discussed in § 6, and for a similar value of the fault slip, the steeper-dipping plane could be expected to result in larger vertical displacements and thus, generally speaking, give rise to a local tsunami of larger amplitude. For this geometry, however, we note that the azimuth of the general direction of rupture separating the main shock from the 09.10 aftershock is oriented at a substantial angle (22°) from the strike of the plane, in the down-dip direction. It is then difficult to map the aftershock on

the fault plane, as one would generally expect, without sinking its focus considerably (several tens of kilometres) along the steeply dipping plane. On the other hand, along the shallow-dipping plane, this problem is largely non-existent and, if anything, would contribute to placing the aftershock up-dip (by a few kilometres) from the hypocentre of the main shock.

Another classical means of distinguishing between fault planes is the mapping of aftershocks. Using the technique of Wysession *et al.* (1991), we relocated 43 aftershocks ($m_b \geqslant 4.4$) reported by the NEIC during the remainder of 1998. All relocations had to be performed at a constrained depth of 10 km. Thirty-three well-constrained epicentres define a fault rupture area *ca.* 70 km by 40 km (figure 1), which is essentially identical to the aftershock area defined by McCue (1998) based on NEIC reports and preliminary data from portable stations deployed after 03 August 1998 by the Australian Geological Survey Organization. This large epicentral scatter would favour the shallow-dipping plane as the fault plane.

Hurukawa *et al.* (1999) used bulletin hypocentres published by the Preliminary International Data Center of the Comprehensive Test Ban Treaty to infer large depth variations among aftershocks, favouring the steeply dipping plane. They do not, however, discuss the depth resolution of the method. These authors also presented data obtained from a deployment of three stations by Y. Tsuji (1998, personal communication) during August and September 1998. This deployment suffered from the inaccessibility of the hinterland, resulting in a very flat aspect ratio for the deployed triangle, which gives little, if any, resolution along the polar angle of a cylindrical coordinate system whose axis would be the shore line. In this geometry, hypocentral depths, trading off with distance across the shoreline, are largely unconstrained and the results inconclusive.

3. Post-tsunami land surveys

The post-tsunami survey took place from 2 to 6 August 1998, and its results were reported by Kawata *et al.* (1999). Its principal goal was to obtain a homogeneous set of run-up measurements. The resulting dataset is presented in figure 2. Its main characteristic is the consistent run-up amplitude of 10 m in the devastated area, extending 23 km from Malol to just east of the Arnold River estuary. A maximum run-up amplitude of 15 m was documented at a location in Arop. Outside this zone, the run-up amplitudes fall very quickly, reaching a relatively benign amplitude of 2 m at Serai, where no tsunami damage was inflicted. This results in a steep aspect ratio for the inundation curve plotted in figure 2, as compared to similar graphs in the case of the 1992 Nicaragua or 1994 Java 'tsunami earthquakes' (Satake *et al.* 1993; Tsuji *et al.* 1995).

Note also that the zone of maximum run-up amplitudes is clearly centred along the eastern spit of Sissano Lagoon, at longitude 142.1° E. While this may be controlled to some extent by offshore bathymetry, it remains remarkable that the portion of coast closest to the hypocentre, namely from the Arnold River to the Serai Hills, suffered no significant tsunami damage.

The survey team also sought to investigate effects directly attributable to the earthquake. While those may be difficult to recognize in an area later devastated by the tsunami, we found no major permanent deformation of the shoreline, identifiable for example by subsided or uplifted beaches, the only exception to this pattern

being two rockslides in strongly weathered, quasi-vertical cliffs forming the western boundary of the coastal plain at the Lumber Mill, and fresh rock falls from the cliffs a few kilometres up the coast from that locale. Also, an occurrence of liquefaction was reported at Arop in water-saturated sand. Later field work by McSaveney *et al.* (2000) has suggested subsidence on the order of 30 cm around Sissano Lagoon. The minor character of these static effects underscores the generally low seismic moment of the earthquake, and in particular the absence of a large low-frequency component. They are in contrast to the case of the 1907 earthquake, when a subsidence estimated at 3–5 m doubled the size of Sissano Lagoon (Neuhauss 1911, vol. 1, pp. 26 and 66).

(*a*) *Interviews with survivors*

In the absence of local tidal gauges, the exact timing of the arrival of the tsunami was not recorded instrumentally, and thus, extensive interviews with survivors were conducted, notably by one author of the present paper (Davies 1998). In this respect, the occurrence of the main aftershock (the 09.09–09.10 doublet, which was widely felt along the coast) provides a natural benchmark for the timing of the arrival of the tsunami: in the context of a major disaster, it is difficult to expect witness reports to provide an accurate quantitative estimate of the time separating, for example, the occurrence of the mainshock from the arrival of the tsunami at a given shore. On the other hand, relative timing should be more reliable: the consensus emerging from Davies's (1998) interviews and the analysis of Imamura & Hashi (2000) is that some of the coastal areas (Malol; see figure 1) experienced two strongly felt seismic events, with the tsunami arriving very shortly after the second one, while at other locations (Arop, Warapu), only one earthquake was reported to be strongly felt, which would suggest that the second strongly felt shock occurred during the devastation of these localities by the tsunami, or very shortly thereafter. In addition, several witnesses report feeling a weak tremor, prior to the two stronger ones; this possible foreshock is resolvable neither in the seismic data, nor in the hydroacoustic records (see § 5). The values of the short-period magnitudes m_b (5.9 at 08.49; 5.6 at 09.09 and 5.9 at 09.10, but only 4.4 at 09.02) then indicate that the two 'strongly felt' earthquakes (in some areas, the second one reported stronger), must be the mainshock at 08.49 and the 09.09–09.10 combination, whose 30 s separation is too short to be resolved in a human report. In particular, the second felt earthquake cannot be the 09.02 event.

We can then interpret the witness reports (Davies 1998) as meaning that the tsunami reached the central part of the devastated zone (Arop, Warapu) at about 09.09, and its southernmost portion at Malol not before 09.11 GMT. This is an extremely important result, because it rules out the main shock at 08.49 as a possible cause of the tsunami: as will be discussed in more detail in § 6, the probable fault area of the mainshock is simply too close to the shoreline to involve a 20 min propagation to Sissano Lagoon. On the other hand, from a simple causal argument, the main aftershock occurs too late to be a plausible source.

Finally, the direction of arrival of the tsunami wave was established qualitatively from survivor interviews, and the mapping of debris paths along the immediate coastal areas. The emerging pattern (Davies 1998) is that of a wavefront essentially parallel to the shore at the centre of the devastated zone (at Arop), but moving sideways at its extremities (westward at Sissano Villages, and southeastwards at Malol). This observation, and the absence of tsunami devastation at Serai, would also tend to rule out the epicentral area of the mainshock as the source of the tsunami.

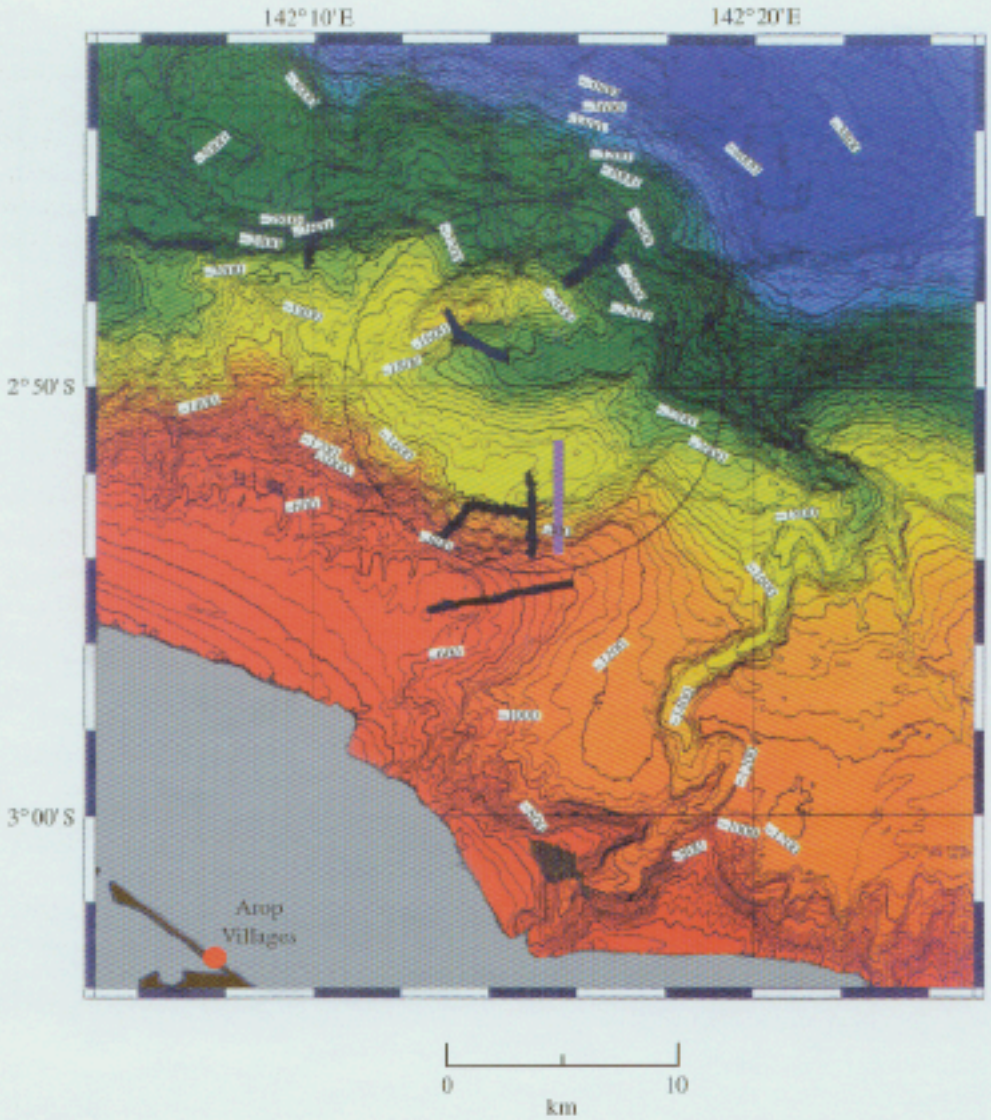

Figure 3. Close-up of the bathymetric data acquired by RV *Kairei* (after Tappin *et al.* 1999), showing (inside the large circle) the amphitheatre where the slump was documented by the dives of *Dolphin* (tracks shown as thick black lines). The purple bar is the location of the cross-section in figure 4. Note also the canyon offshore Malol, to the southeast. Isobath interval 50 m. Data were collected by a SeaBeam 2112 multibeam survey system capable of wide swath mapping and side-scan imaging using multiple 12 kHz acoustic beams. Sissano Lagoon is at the lower left, with the eastern spit shown. The grey area is the domain shallower than 200 m, for which no bathymetric data are available.

4. Marine surveys

As described in detail by Tappin *et al.* (2001), marine surveys were carried aboard RV *Kairei* (KR9813) in December 1998 and RV *Natsushima* (NT9902) in January

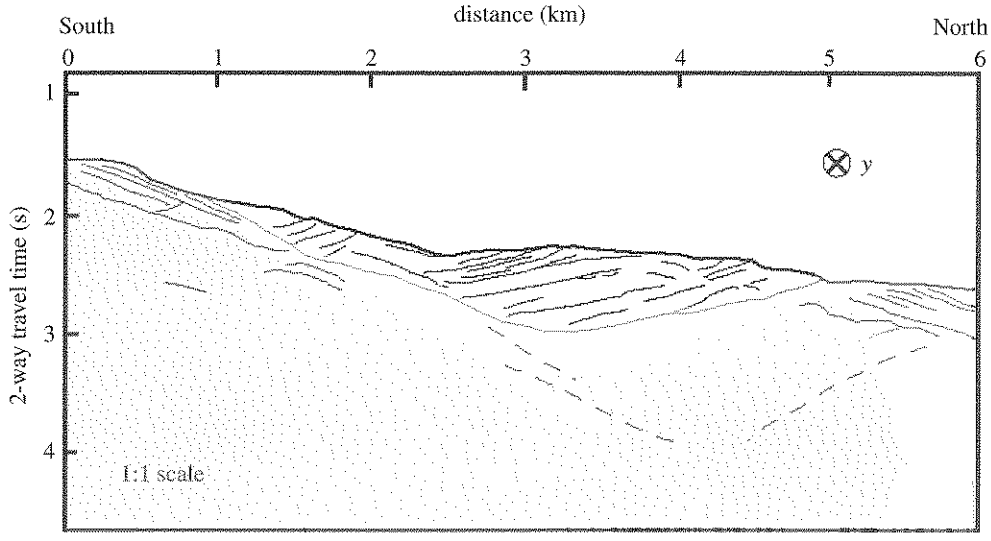

Figure 4. Interpretative sketch obtained from a seismic reflection transect midline through the slump (purple line in figure 3), drawn without vertical exaggeration. The symbol at upper right identifies the direction y used in estimating the transverse extent of the slump (see § 6). The slump is shown in white, with the basement rock in grey. We obtained seismic records with a high-resolution GI gun sound source and a 1200 m long digital hydrophone streamer towed behind the vessel. Shot and hydrophone spacing were both 25 m, yielding 24-fold stacking of the reflected waves. We migrated the temporal data using a Stolt (F-K) algorithm and SIOSEIS seismic processing software.

1999. Figure 3, adapted from Tappin *et al.* (1999), shows the resulting offshore bathymetry. The most interesting feature revealed by the survey was the presence of a large arcuate amphitheatre centred at 2.83° S, 142.26° E, bounded at its northern end by an uplifted block at 2.80° S, 142.22° E (circle in figure 3). To the north of the raised block a fault was identified consistently over a length of 40 km. During the cruise of RV *Natsushima*, the ROV *Dolphin* was deployed for six dives, whose tracks are shown as the thick black lines in figure 3, and which returned visual evidence of strong, recent, ground motion on the walls of the amphitheatre, as documented by the presence of fresh headwalls, near-vertical cliffs, brecciated blocks, fresh fissures in cohesive sediments, and basement faulting between these geological features (Tappin *et al.* 2001). By contrast, evidence of recent movement along the 40 km fault was found only in its western section, making the structure an unlikely candidate for the source of the tsunami (Tappin *et al.* 1999). Finally, in the southern part of the amphitheatre, a mound *ca.* 100 m in height was mapped, and visually interpreted as the result of recent slumping of a cohesive block, involving deep rotational failure in stiff clay. At this stage of the investigation, the fresh nature of the slump made it a possible, if not yet probable, source of the tsunami.

The area was visited again in September 1999, this time by RV *Maurice Ewing*, which conducted high-resolution seismic reflection surveys along a series of profiles including a north–south cross-section of the amphitheatre and slump body. Figure 4 shows a seismic reflection transect along the profile drawn in purple in figure 3; it images the internal structure of the underwater slump (Sweet 2000; Sweet & Silver

2002). A shallow depression along the upper slope *ca.* 100 m deep and 750 m long coincides with the headwall observed by *Dolphin*. A basal failure plane is clearly imaged to a maximum depth of *ca.* 600 m below the sea floor (0.7 s two-way traveltime). The failure plane appears to curve toward the surface farther to the north, with the curvature supported by back tilting of strata within the thickest part of the slump (figure 4). The tilted layers are parallel, precluding growth of the structure through time and suggesting largely coherent motion. The sea floor outcrop near the toe of the basal detachment coincides with a steep escarpment, *ca.* 100 m high, located 4.5 km north of the head scarp. A rough reconstruction of the original mass position suggests a vertical centre-of-mass drop on the order of 380 m (Sweet & Silver 2002).

The results provided by the three marine surveys thus offer compelling evidence for fresh geological activity in the area of the amphitheatre and on the western end of the 40 km fault, and in particular for the occurrence in the presumed source zone of the tsunami, of a massive slump whose volume is estimated at 4 km^3 in § 6 below. The surveys remain, however, powerless regarding the exact timing of the slumping event.

5. Hydroacoustic data

Documented underwater slides have been detected historically using cable breaks (Doxsee 1948), and a few aerial slides have had their seismic records studied extensively, notably the landslide associated with the explosion of Mount St. Helens on 18 May 1980 (Kanamori *et al.* 1984). If the slump surveyed by the shipboard expeditions failed in association with the PNG earthquake, and in the absence of reported breaks in underwater cables, its signature should be detectable in the geophysical record. Ideally, we look for an event occurring in the time-interval between the mainshock, which at 08.49 GMT is too early to be a plausible source of the tsunami (see § 3), and the main aftershock at 09.09, which is too late. Two obvious candidates are the aftershocks reported by the NEIC during that time window, i.e. the 09.02 and 09.06 events. In this section, we provide evidence suggesting that the 09.02 aftershock was an underwater slump, and cast it as the most probable origin of the tsunami. We note first that our seismic relocation of the 09.02 aftershock yields an epicentre at 2.85° S, 142.10° E, and a 1 s Monte Carlo ellipse covering the amphitheatre in its easternmost part (figure 1). The ISC location (2.87° S; 142.11° E) is essentially the same as ours, and while their error ellipse is slightly smaller than ours, it similarly intersects the amphitheatre. It is then legitimate to place the event in the cavity.

Unfortunately, there exist few if any detailed seismic records of the PNG sequence at short epicentral distances. The closest available seismic record, at Port Moresby (900 km), suffers from high background noise levels. For this reason, we investigated the characteristics of the T waves (Brekhovskikh & Lysanov 1991) recorded on hydrophones and at Pacific shore seismic stations. Figure 5 shows that the coastal geometry of New Guinea and the Admiralty Islands results in blockage towards a large portion of the Pacific Basin, but we were able to obtain excellent records at several locations. In figure 6, we study hydrophone records at Station WK31, southeast of Wake Island, 3600 km from the epicentre. The top frame (*a*) shows a 120 s time-series and corresponding spectrogram of the T wave generated by the 09.02 aftershock. Note that it lasts *ca.* 45 s, thereby approaching the duration of the main-

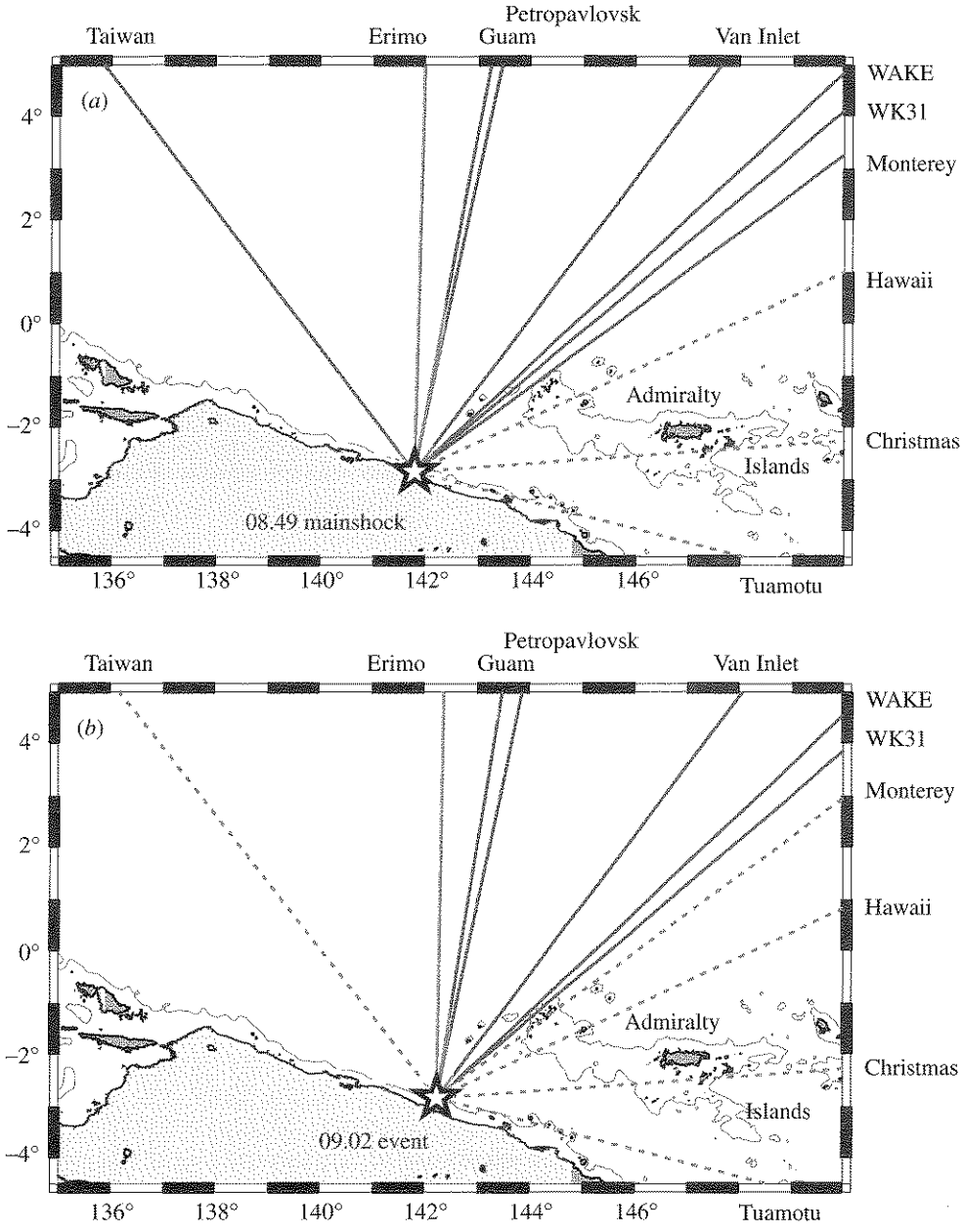

Figure 5. Blockage of T waves from the PNG epicentral areas to various sites in the Pacific. The only isobath plotted is at 1200 m, characterizing the axis of the low-velocity SOFAR channel, using the bathymetry of Smith & Sandwell (1997). T-wave great circle paths are plotted from the epicentre of the mainshock (08.49 GMT; top frame (a)) and from the centre of the amphitheatre (bottom frame (b)), as solid lines if the acoustic wave was recorded, as dashed lines otherwise. This bathymetry explains blockage by the Admiralty Islands of direct rays to Hawaii, Christmas and the Tuamotu Islands, as well as to the Monterey OBS for the 09.02 event. It cannot, however, explain the lack of recording of the event in Taiwan.

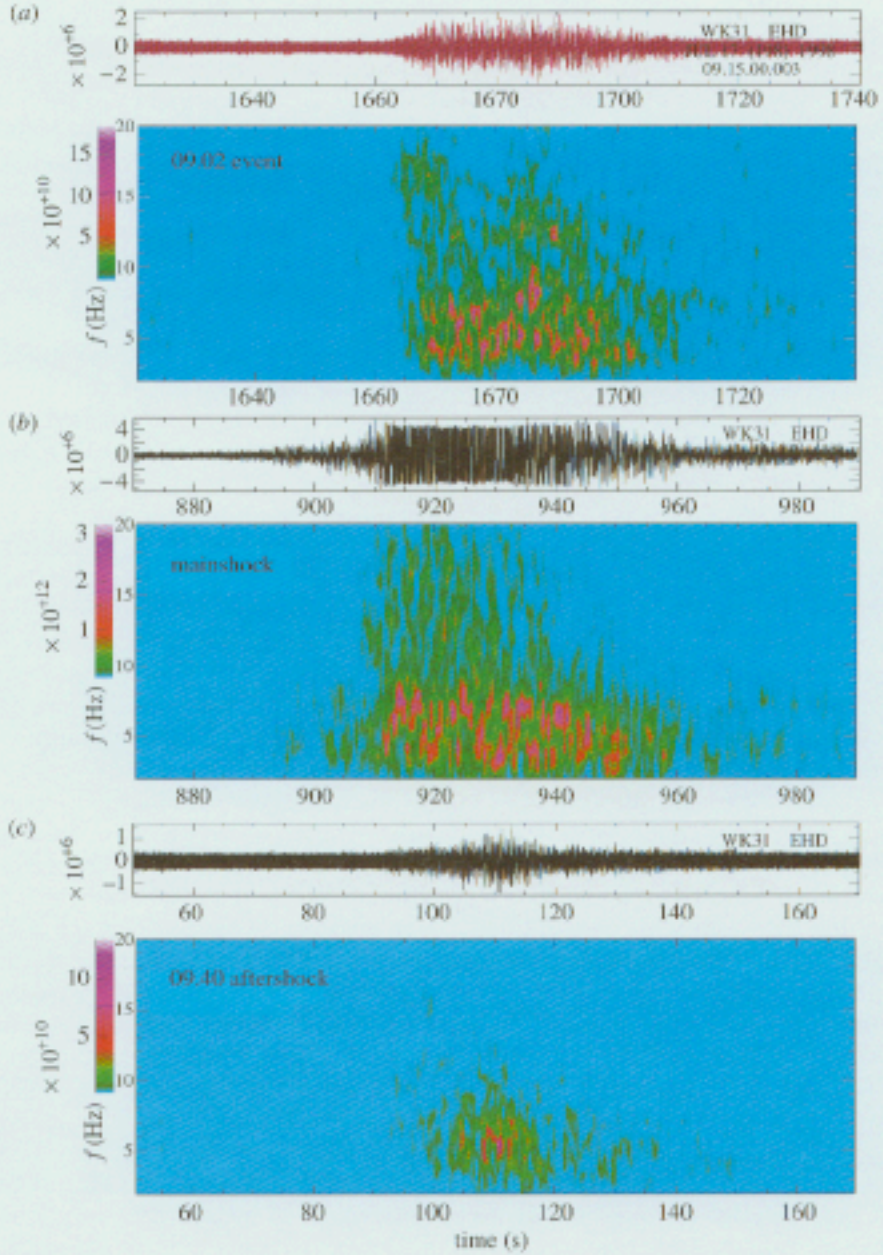

Figure 6. Time-series and spectrograms of T waves received from the PNG sequence at the hydrophone station WK31 of the PIDC. All time-series are 120 s long. The 09.02 event ($m_b = 4.4$) interpreted as the tsunami-generating slump is shown at the top (*a*), and compared to the mainshock (*b*) and an aftershock at 09.40 (*c*), with similar magnitude ($m_b = 4.5$) and location. The spectrograms contour the energy present in the signal as a function of time (abscissa) and frequency (ordinate). Note the exceptional duration (45 s) of the 09.02 signal. The duration of the mainshock T wave is not affected by the obvious amplitude saturation of the signal.

shock signal (*ca.* 55 s; frame (*b*)). Such a duration is irreconcilable with the source process of a regular $m_b = 4.4$ earthquake, as demonstrated by the T wave from the 09.40 aftershock ($m_b = 4.5$; frame (*c*)). Note also the strong peak in frequency at 8–12 Hz, half-way into the duration of the signal. The exceptional duration of the 09.02 T wave, and the significant high-frequency components in its spectrum indicate that its source process is more complex than the simple rupture expected for a classical earthquake dislocation of that magnitude.

These results are supported (Okal 1999) by observations at seismic stations on the island of Wake, at Petropavlovsk (Kamchatka), Erimo (Hokkaido), Guam, Van Inlet (Canada), and possibly, following reflections, at Molokai, Maui, and Christmas Island. We were, however, unable to detect any signal associable with the 09.02 event at Pin-lang (Taiwan), and the Monterey Bay Underwater Observatory, both sites where the mainshock T wave is well recorded. Blocking to Monterey can be explained by the eastward location of the source, relative to the mainshock, for which the ray hits the western end of the Admiralty Islands (figure 5*b*), but the global bathymetry used for figure 5 (Smith & Sandwell 1997) cannot explain the lack of signal in Taiwan. This calls for a different nature of source-side masking for the 09.02 aftershock. An acoustic source located on the sea floor inside the amphitheatre-shaped cavity mapped by *Kairei*, with its relatively rigid lateral walls protruding into the SOFAR channel, could generate highly directional T waves, restricted in azimuth to the direction open to the high seas (mostly NE), and blocked at the source towards Taiwan.

As for the frequency characteristics of the T wave, they show a source rich in high frequencies (8–12 Hz), which develop *ca.* 20 s into the signal. This would argue for an accelerated source, as would be expected from a developing slump.

We also examined the question of whether the 09.02 event could actually represent the impact of the tsunami on the coast, which might conceivably be expected to contribute both a seismic and a hydroacoustic signal. We rule out this interpretation on two counts: first, the seismic epicentre remains too far north, its error ellipse not intersecting the shore (figure 1); and second, the pattern of hydroacoustic masking to Taiwan could not be explained. Rather, if the tsunami hits the shoreline during the 09.09–09.10 aftershock, any contribution it may have to the seismic or hydroacoustic spectrum will be drowned into the background of that double aftershock.

Finally, we address the question of the uniqueness of the T-wave record in figure 6*a*, by considering all PNG aftershocks occurring during the remainder of the (GMT) day 17 July 1998. In addition to the 09.02 aftershock, there are 42 such events reported by the NEIC, with maximum magnitudes (apart from the 09.09 and 09.10 shocks) $m_b = 4.7$. Of those, six did not generate T waves recordable at WK31 and one (at 11.28.51) took place during a gap in recording. Of the remaining 35, only four have T waves at WK31 lasting between 37 and 47 s, a duration comparable with that of the 09.02 event; however, their spectral amplitudes are all at least one order of magnitude lower. All remaining events (including the 09.06 aftershock which was, in terms of timing, a potential candidate for the source of the tsunami) have 'regular' T waves, lasting 15–25 s, and generally comparable with those of the 09.40 aftershock (figure 6*c*). In addition, we recognized at least two dozen T-wave signals unassociated with NEIC epicentres, but sharing the general shape of the associated waves. The four T waves of long duration are associated with (i) the 09.29 event (relocating at the western end of the mainshock rupture), part of a long, complex series of

puffs extending over more than 300 s, but the only one among them lasting more than 20 s; (ii) the 10.51 shock (sharing its epicentre with the 09.02 event), whose T wave lasts 37 s but with highest frequencies (7 Hz) concentrated in the earliest part of the signal, thus arguing against generation by an accelerating sliding motion; (iii) the 12.15 event (which could not be meaningfully relocated), but whose T-wave duration of 37 s, and maximum frequency of 8 Hz occurring towards the centre of the record, make it closest in properties to the 09.02 slump; and (iv) the 13.52 aftershock ($m_b = 4.5$), relocating north of Malol in the Canyon surveyed by *Kairei*, and which could have triggered a small episode of slumping along its walls.

Thus, the 09.02 event appears unique (at least on that particular day) from the standpoint of its amplitude, rather than from its characteristics of duration and frequency spectrum, which are approached, if not exactly duplicated, by a handful of events. On this basis, we propose that the slump evidenced by the ROV *Dolphin* and profiled by Sweet *et al.* (1999) took place at 09.02 GMT on 17 July 1998, and generated the tsunami. The other T waves of long duration but much smaller amplitude would correspond to secondary rockslides or slumps that would be expected to take place on the steep slopes along the rupture zone of the main shock. Only the 09.02 slump had the size and power necessary to generate a substantial, lethal tsunami.

This interpretation remains tentative on several accounts. First, and in the absence of clear insight into the mechanism of generation of the acoustic wave, it is difficult to locate precisely the origin of the 09.02 T waves, beyond the crude observation that their arrival time patterns at the various stations are in agreement with those of the mainshock and other aftershocks. In addition, little is known regarding transoceanic T waves generated by documented underwater slumps: the 1975 Kalapana event was obviously much larger (see discussion below), whereas the 1975 Kitimat, BC, and 1994 Skagway, Alaska slides or slumps occurred at the back of fjords (Murty 1979; Kulikov *et al.* 1996), and could not radiate acoustic energy into the wide ocean. The duration of the PNG slump, estimated at 45 s from the hydroacoustic records, falls short of the 30 min or longer reported for the Grand Banks or Kalapana events, even taking into account the latter's much larger sizes. We interpret this duration as expressing the absence of a turbidity current, which in turn is probably due to the containment of the slide inside the existing amphitheatre.

6. Computer simulation of the PNG tsunami

(*a*) *The failure of the earthquake source*

In this section, we first attempt to model the observed run-up distribution by simulating the generation of the tsunami from the coseismic displacement induced by the shallow-dipping thrust fault mechanism (strike 146°; dip 19°; rake 127°) of the Harvard CMT inversion (Dziewonski *et al.* 1999). As a worst-case scenario, we use the larger seismic moment initially published as the 'QUICK CMT' Harvard solution (5.2×10^{26} dyn cm) as opposed to the final, lower value of 3.7×10^{26} dyn cm. The characteristic slip along the rupture plane is taken as 1.06 m, and the rigidity as 58 GPa, with rupture propagating at 3 km s^{-1} in the azimuth N85° E. The vertical displacement of the ocean floor is computed by adapting the half-space model of Mansinha & Smylie (1971) to the case of a rupture propagating at an angle from the direction of fault strike, in a geometry sketched in figure 7. The hypocentral depth at the initiation of rupture is taken as 17 km, and the slight up-dip propagation results

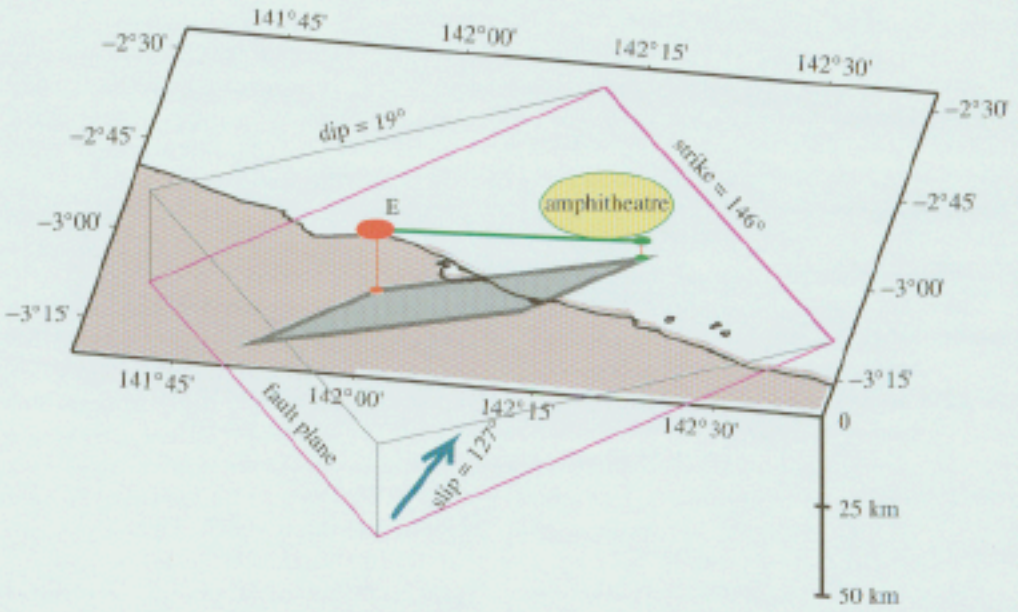

Figure 7. Three-dimensional sketch of the geometry of rupture used in the modelling of the tsunami as a seismic dislocation. The fault plane is shown in purple, with its intersection with the surface (at a strike of N146° E) as a heavier purple line. The zone of rupture is shown as the grey area on the fault plane. We use our relocated epicentre (large solid red dot, 'E'), and an initial depth of 17 km (smaller red dot). The rupture propagates at an angle with the fault strike, resulting in a slightly up-dip motion, ending at the northeastern corner of the fault zone (green dots). The green line is the surface projection of the rupture. The amphitheatre is shown by the yellow disc. The blue-green arrow is the orientation of the slip vector, and represents the motion of the hanging (Australian) block over the foot (Caroline–Pacific) one. The rupture area is 910 km^2, and the amplitude of slip 1.06 m.

in a final depth of 4.8 km at the shallowest extremity. By transposing vertical sea floor displacement instantaneously to the free surface, we arrive at an initial maximum tsunami amplitude of 40 cm (figure 8). Note that this displacement agrees with the vertical offset observed along basement faults during ROV dives in the source region.

Our simulations then yield a peak run-up of 1.3 m along the affected shoreline (figure 8), 7–8 min after the mainshock. Even accounting for a possible factor of 2 in the (largely unknown) response of the beach site, it is clear that such a wave would have remained benign even at its point of maximum amplitude. Furthermore, figure 8 shows that the lateral decay of the amplitude of the wave along the coastline is weak, and does not match the observed spatial concentration of the wave around Sissano Lagoon. Finally, under this model, the tsunami would have been early, reaching Malol at least 12 min *before* the main aftershock at 09.09–09.10 GMT. At this point, we must underscore that any dislocation source occurring in the same general region as modelled above, will suffer the same failure to match the arrival time of the tsunami, as long as it remains coseismic with the mainshock at 08.49 GMT.

More generally, a source coeval with the mainshock could fit the reported arrival times at the shore only if the propagation of the tsunami took at least 12 min longer.

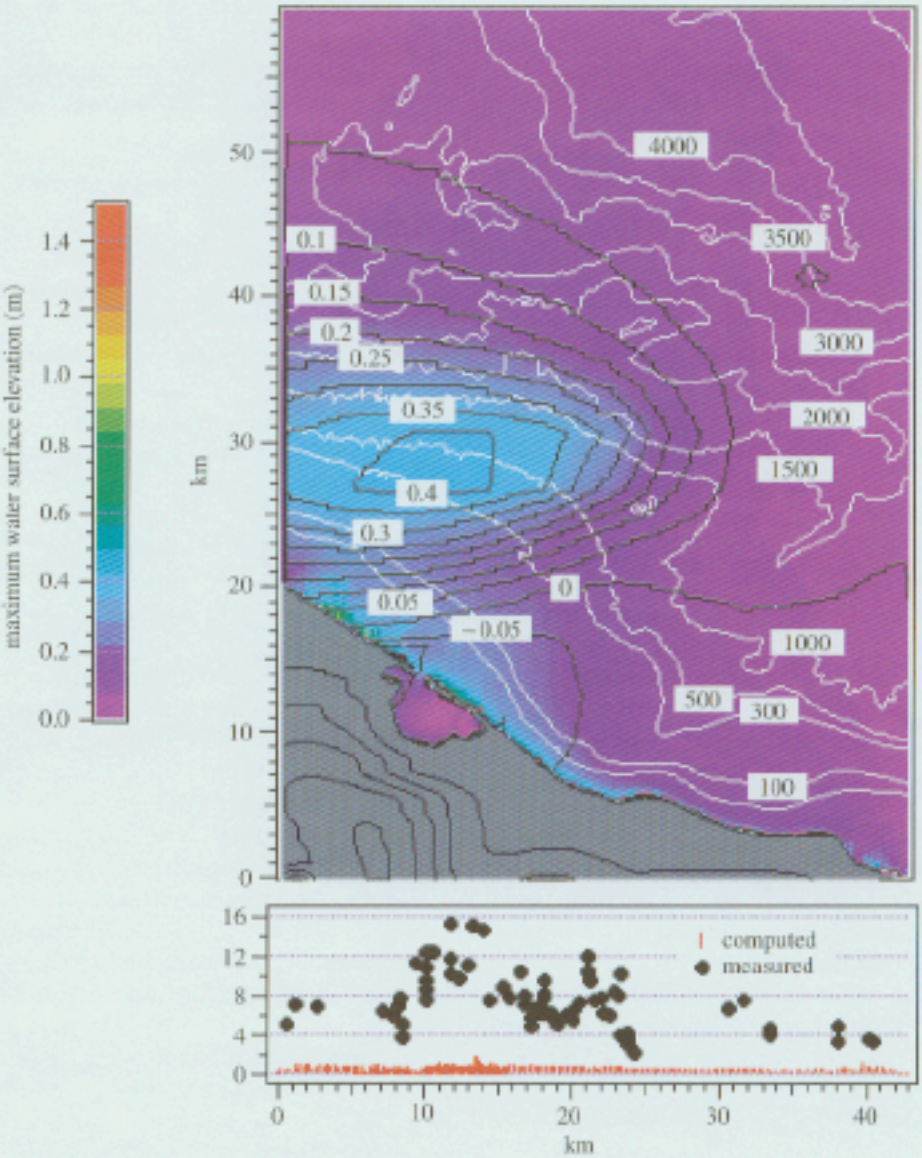

Figure 8. Top: computed tsunami waveshape resulting from the mainshock. The white contours are isobaths (labelled in metres from 100 to 4000 m). The black contours show the static deformation inferred for the dislocation model sketched in figure 7, labelled from −0.05 m (subsidence) to +0.40 m. The shaded colours represent the field of maximum positive amplitude at the surface of the sea reached during the 1000 s following the start of the simulation (see scale bar at left). Bottom: maximum computed run-up near Sissano Lagoon (red bars), compared with measured values (black dots). The darker central section results from the use of a denser grid. Our results yield run-up of negligible amplitude, and spread over a large segment of coastline, peaking 7–8 min after the mainshock.

In principle, this could be achieved in two ways: by constraining the propagation to the continental shelf (in practice requiring the wave to propagate 30 km *along* the coastline from the epicentral area at Serai), but this would fit neither the westward flow of the wave at Sissano Villages, nor the rapid decrease of the run-up heights west of Sissano; or by moving the source of the tsunami in a direction normal to the shoreline. However, moving the tsunami source out to sea results in a significantly greater incremental velocity (because of increased water depth). We note in figure 8 that the largest amplitude of the initial wave takes place in water *ca.* 1000 m deep. Using this value as a very conservative minimum depth over which the incremental propagation must take place, we find that the source must be 70 km farther out at sea to delay the tsunami by 12 min. This is clearly unacceptable from the standpoint of both the seismological data and the structural observations by *Dolphin*, and this argument should be enough to rule out the mainshock as the source of the tsunami in any conceivable geometry of rupture.

However, and because of the qualitative nature of the timing constraint, we discuss here possible variations to the dislocation source which may enhance the tsunami excitation. In order to bring the maximum amplitude of the flow depth across the shore line to an acceptable value (which we take as 5–6 m to account for the possible run-up response of the beach site), we would need at least 9 m of slip along the shallow-dipping fault plane, which cannot be accommodated by an earthquake of only 5.2 (more realistically 3.7) $\times 10^{26}$ dyn cm without incurring a strain release of at least 2×10^{-3}, which is unacceptable in crustal rocks.

A number of authors, notably Tanioka & Ruff (1998), have argued that the steeply dipping plane may provide a greater vertical motion, and hence a larger tsunami, for the same value of the seismic moment. Matsuyama *et al.* (1999) have recently detailed this argument by using a 40 km eastwards propagation geometry similar to Kikuchi *et al.*'s (1998), and located 25 km north of Sissano, i.e. along the 40 km fault defined during the *Kairei* cruise, a model also advocated by Geist (2000). They use a maximum initial water height of 1 m to obtain run-up amplitudes of *ca.* 7 m along the spits of Sissano Lagoon. There are, however, several problems with this model (Okal & Synolakis 2001): as explained in § 2, propagation on a steep plane at an angle to its strike involves a substantial down-dip component, reducing the sea floor deformation. Also, the *Natsushima* survey has revealed that fresh movement on the 40 km fault is limited to its western section and is of normal, rather than thrust, polarity (Tappin *et al.* 1999). Finally, Matsuyama *et al.* (1999) propose to circumvent the timing inconsistency by assuming that the tsunami was generated by the main 09.10 aftershock; however, the latter is not only too late to be the source of the wave (see discussion above), but also one full unit lower in mantle magnitude M_{m} than the main shock, which further rules it out as a possible generator of the tsunami.

A second class of studies (Tanioka & Ruff 1998; Tanioka 1999; Satake & Tanioka 1999) has focused on teleseismic recordings of the tsunami. The second and most detailed study concludes that the steep reverse fault explains the tsunami waveforms 'slightly better' than the shallow dipping one. In this respect, it must be borne in mind that the modal theory of tsunami excitation (Ward 1980; Okal 1988) predicts that it is theoretically impossible to discriminate on the basis of tsunami waves between the two fault planes of a point source seismic dislocation, or in practice when the size of the rupture (at most 35 km in the present case) becomes small

with respect to both tsunami wavelength and distance travelled. In addition, as discussed above, and because of the shorter wavelengths it generates, a slumping source is expected to contribute only minimally to the far-field tsunami, so that the tidal gauge data in the far field provide essentially no resolution of a slump source. Finally, Tanioka's (1999) preferred model ('B') has the rupture area only 10–15 km from Sissano Lagoon, which would result in an even earlier arrival of the tsunami wave at the shore.

Satake & Tanioka (1999) later proposed a composite model in which the low-angle thrust fault triggers a splay fault in the accretionary prism. This model is reminiscent of the geometry proposed by Fukao (1979) to interpret 'tsunami earthquakes' observed to follow major shallow-angle interplate thrust events (e.g. Kuriles, 20 October 1963; 10 June 1975). Rupture at very shallow depths in mechanically weaker material could enhance tsunami excitation (Okal 1988), but any substantial fraction of moment release in such material would bring a significant non-double-couple component to the best-fitting moment tensor. Departure from a pure double-couple solution can be expressed through a so-called compensated linear vector dipole coefficient ε (Jost & Herrmann 1989). The PNG earthquake features $\varepsilon = 0.08$, actually smaller than the average value (0.12) of $|\varepsilon|$ for the entire CMT catalogue; in other words, there is no evidence for a composite mechanism in the source of the mainshock. On the other hand, and although the authors do not address the question of timing, it is conceivable that a 13 minute gap could separate rupture on the two parts of the fault. But then, the seismic moment necessary to generate the tsunami, even in a mechanically weak accretionary prism, would give the 09.02 seismic event a magnitude larger than $m_b = 4.4$. Also, the shallow splay fault would be expected in the area of the 40 km fault, where fresh motion, if any, is of the wrong polarity.

The conclusion of this section is then that we cannot find a model of seismic dislocation for the generation of the tsunami which would be compatible with the full set of available seismological observations, with morphological and structural observations from the shipboard surveys, and with the timing of the wave at the shore, as reconstructed from survivor interviews.

Finally, we wish to emphasize that all the modelling in this section was performed in a worst-case scenario, using the overestimated moment of the Harvard 'QUICK' solution, and the shallowest available estimates of the hypocentre. The maximum amplitude computed, 1.3 m, must therefore be regarded as an upper bound of the tsunami wave actually generated by the dislocation source of the main shock. The mainshock must have generated a small local wave, but at a height of 1 m or less, it could have gone largely unnoticed along sections of the coast featuring a natural berm of that height above the high-water line.

(*b*) *The 09.02 slump as the source of the tsunami*

In this section, we model the tsunami as generated by an underwater slump, in the geometry determined by the shipboard surveys, and taking place at 09.02 GMT, based on the hydroacoustic evidence described in § 5. Modelling tsunami generation by submarine mass failures remains a complex undertaking, which must first involve the dynamic description of the slumping itself. For example, Jiang & LeBlond (1992) developed depth-averaged wave equations by representing submarine mass failures as volumes of immiscible fluid with uniform density and viscosity; Pelinovsky &

Poplavsky (1996) presented a simplified model for tsunami generation using elegant velocity potential solutions for a moving Rankine ovoid at the sea floor; Ward (2001) used the Green's function to a three-dimensional linear wave equation and calculated the free-surface evolution of the waves from complex landslides; Heinrich (1992) and Grilli & Watts (1999) have developed potential flow fluid dynamics models of the tsunami generation region. Watts (2000) modelled landslides and slumps as solid block slides using a combination of Gaussian profiles and scaling parameters derived from laboratory experiments; these scaled initial conditions have been tested specifically using the PNG slide by Watts *et al.* (1999), and also used by Tappin *et al.* (2001).

In this context, we first note that geological evidence suggests a cohesive behaviour for the slump, as documented for example by the stiff biogenic mud revealed in a push core taken by *Dolphin* along the exposed failure plane (Tappin *et al.* 2001). Similarly, sub-bottom profiles and seismic records of slumped material show failure planes lacking significant internal deformation (Sweet *et al.* 1999; Sweet 2000), indicating that the main mass of cohesive sediment did not break into separate blocks. In this framework, and based on available bathymetric and seismic data, combined with ROV observations, we use for the slumping block a length of 4.5 km, a width of 4 km, and a total thickness of 600 m (figures 3 and 4). Assuming parabolic profiles across both width and length, we thus estimate the volume of the slump at $4\,\mathrm{km}^3$ of sediment, a relatively modest figure by geological standards, which have been reported to exceed $1000\,\mathrm{km}^3$ (Prior & Coleman 1979; Hasegawa & Kanamori 1987; Eissler & Kanamori 1987; Schwab *et al.* 1993; Turner & Schuster 1996). This figure is in agreement with the estimate of the slump's volume given by Sweet & Silver (2002). It is noteworthy that the PNG slump is comparable in volume to the Mount St Helens aerial avalanche, perhaps the best seismologically studied landslide source (Kanamori *et al.* 1984). However, the latter produced a much larger long-period seismic signal, presumably due to the difference in effective mass and slope (Seed *et al.* 1988), and perhaps to the containment of the slump inside the PNG amphitheatre.

Once the dimensions of the slump are modelled, we use the scaling relationships of Watts (2000), with a translation distance of *ca.* 1 km along the failure plane. Given the 4:1 aspect ratio of slump width to ocean depth, we do not model three-dimensional effects during wave generation, and the transverse tsunami profile is simply represented by the function $\mathrm{sech}^2(3y/(w+\lambda))$, where $w = 4\,\mathrm{km}$ is the slump width, λ is the characteristic wavelength (here 4.4 km), and y is measured perpendicular to the transect (figure 3), as per Watts *et al.* (1999).

This is as an ad hoc choice proposed by Watts *et al.* (1999) to allegedly balance transverse generation and propagation effects. To our knowledge, no validated models exist that can predict the evolution of the free surface in the transverse direction after a slide, given only a two-dimensional transect, such as presented in figure 3. Furthermore, even if sophisticated three-dimensional wave evolution models did exist, their use would presume the knowledge of the evolution of the slide based on soil properties before the event, and of details of the bathymetry. Hence, their application in this context would have been specious, for it would imply knowledge of field data that are not available. Also, recently, Lynett & Liu (2001) have presented a Boussinesq model that is computationally efficient for solid block slides, and their results suggest that the shape of the block does affect to first order the evolution

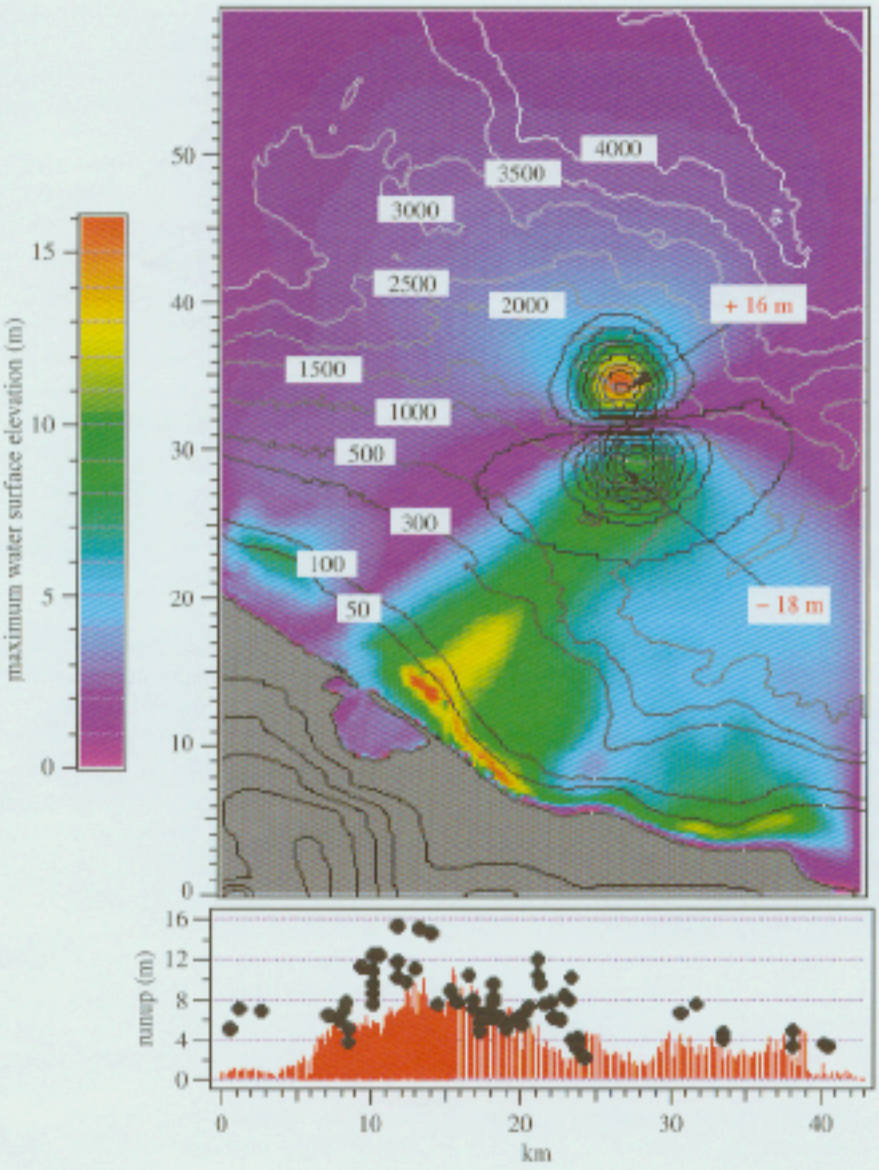

Figure 9. Top: computed tsunami waveshape for the slump model. This figure is similar in concept to figure 8, with the black contours (2 m interval) showing the shape of the sea surface 44 s after the beginning of the slumping event, when the simulation is started. The field of colour-shaded maximum amplitudes is superimposed (scale bar at left). Note the onslaught of a wall of water concentrated on the Malol-to-Sissano area. Bottom: maximum computed run-up along coast line (red bars), compared with measured values (black dots). Note the overall agreement in amplitude and shape.

of the water surface. This notwithstanding, Synolakis *et al.* (2000) have used eighteen before-and-after-event bathymetric transects over *ca.* 1 km to model the 1994 Skagway, Alaska tsunami, and found that the simple method used here does produce results consistent with eyewitness observations. Finally, for nearshore slides, we have found that, while the regional maximum run-up is affected by neither the transverse propagation nor the orientation of the initial slide within reasonable ranges, the distribution of maximum run-up values can be.

The final step consists of feeding the two-plus-one-dimensional tsunami waveshape into the tsunami propagation and run-up model of Titov & Synolakis (1998), who solve the nonlinear shallow water wave equations as a system of hyperbolic differential equations able to simulate overland flow by extending the simulation domain. Their model has been shown to correctly predict even the extreme run-up observed in 1993 at Okushiri, Japan, in the case of a tsunami generated by a dislocation source, for which accurate before and after bathymetric profiles are available. The top part of figure 9 shows the dipolar nature of the initial field of sea surface displacements, which will give rise to large amplitudes in the near field, but contribute very little in the far field, as suggested by Tadepalli & Synolakis (1994, 1996). The particular profile used here is the same as in Tappin *et al.* (2001) and Borrero *et al.* (2001). The symmetry of the dipole reflects the fact that the structure of the slump remains cohesive during its motion, and does not decompose into a turbidity current (Heinrich *et al.* 2000).

The bathymetric data used in the simulation is as mapped by *Kairei* for depths greater than 400 m, interpolated from the shoreline to a depth of 150 m based on local marine charts, and interpolated between those two sources for intermediate depths. On-land transects made by the ITST (Kawata *et al.* 1999) provided topography around Sissano Lagoon. As discussed by Kanoğlu & Synolakis (1998), wave interactions with a coastline are most affected by the shallowest regions and consequently all PNG simulations remain somewhat tentative. For this reason, we employed a grid spacing of 200 m. Also, in the particular case of figure 9, we have used a uniformly sloping beach behind the spit, in agreement with the work of Borrero (2002), who determined that in this particular geometry, computing flow depths at the overtopping point using a sloping beach produces more physically realistic results than modelling the entire evolution past the spit, possibly due to the complex dynamics of breaking that most likely took place as the wave approached the spit.

7. Discussion and conclusion

As shown in the bottom frame of figure 9, the fundamental features of our run-up simulations compare favourably with the dataset of field measurements.

(i) In clear contrast to the case of the dislocation source, the shape of the amplitude profile along the coast is adequately reproduced by our model, with maximum heights concentrated along the portion of coastline between Malol and Sissano. The detailed wavefield on the map portion of the figure illustrates dramatically the wall of water approaching the Arop–Sissano area.

(ii) The amplitude modelled along the coastline from Sissano to Malol averages 8–10 m. This is less than the extreme values measured at Arop (15 m) and Malol (up to 12 m), but remains within the range of scatter of the ITST dataset.

Furthermore, the measured run-up values are the result of the interaction of the wavefield with the shallowest portion of the beachfront, where no detailed bathymetry is available, and which could easily explain the 20–50% discrepancy in wave height between observed and modelled values. Along the spits, the computed values are more representative of flow depths than of maximum run-up heights. There is a rather poor fit to the values observed at Arnold River, at the extreme northwestern part of the dataset. The high run-up values measured at that location are probably due to the local interaction of the wave with the estuary of the Arnold River, which is not included in the model.

(iii) Finally, this model explains the timing of the tsunami. We use a time of 09.02.50, corresponding to the final part of the source of the hydroacoustic records, to start the computation of the propagation of the tsunami from the field of sea surface deformation illustrated in figure 9. Tsunami arrival times on the shore are then 09.10 at Malol and approximately 09.12 at Arop. The former is in agreement with Davies's (1998) reconstruction from eyewitness accounts, the latter remains *ca.* 3 min late. However, most of the travel time is spent in the shallow continental shelf, whose bathymetry was not chartered by *Kairei* and could be inaccurate.

In conclusion, our analyses of tsunami amplitude and timing, based on available bathymetric and seismic images, support the scenario of the generation of the PNG tsunami by a large underwater slump at 09.02 GMT. With hindsight, geotechnical analysis would have indicated that slump failure is a distinct possibility for earthquakes in this region. We estimate a mean shear stress of 0.5 MPa and a mean effective overburden of 4.4 MPa along the initial failure plane. From these values, we calculate an average residual undrained shear strength along the initial failure plane for normally consolidated sediment $S_u \approx 0.5$–1.5 MPa that is within the range of accepted values measured for other stiff clays (Bardet 1997); we expect a sediment-starved and subsiding margin to have normally consolidated sediments. The largest peak horizontal acceleration required for an earthquake to induce static failure is $0.5g$, an acceptable value for a magnitude 6.5 earthquake within a 10 km radius of the faulting (Joyner & Boore 1981). The slump was in line with seismic energy release and therefore subject to strong ground motion as demonstrated by ROV investigation of the tsunami source region (Tappin *et al.* 1999, 2001). The delay of 13 min between the mainshock and the initiation of the slump may be attributable to the nucleation of failure in the sedimentary mass.

The PNG event reaffirms, if need be, the significant local tsunami hazard posed by submarine mass failures following earthquakes of even relatively moderate size. At present, it remains largely a single case study, notably because the geophysical signature of underwater slides or slumps in terms of conventional seismic waves is still poorly known. Thus, the question of tsunami hazard assessment, and of an eventual warning prior to a future submarine mass failure, remains rather speculative, although, in the case of well-studied margins, the methodology used in the present study can be implemented in quantitative simulations of tsunami attacks due to submarine mass failure (Borrero *et al.* 2001). In this respect, this approach bears significant promise for tsunami hazard mitigation.

D.R.T. acknowledges SOPAC, JAMSTEC and the PNG Government for organizing two research cruises on short notice. J.C.B., E.A.O., C.E.S., E.A.S. and S.S. were supported by several NSF

programs at various stages of this project. We thank Shun-ichi Koshimura for digitized nearshore bathymetry data, Gary McMurtry for the sediment density analysis of the *Kairei* piston cores, and Abraham Lerman for help with translation. Stefano Tinti provided a careful review of an earlier version of the manuscript. Seismic records were obtained from the IRIS data management centre, the Prototype International Data Center of the CTBT, or kindly provided by Cecily Wolfe (PELEnet), Jesse Williams (MBARI), and Bor-Shouh Huang (Taiwan network). Several figures were drawn using the GMT software (Wessel & Smith 1991).

References

Ambraseys, N. N. 1960 The seismic sea wave of July 9, 1956 in the Greek archipelago. *J. Geophys. Res.* **65**, 1257–1265.

Bardet, J.-P. 1997 *Experimental soil mechanics.* Prentice Hall.

Bjerrum, L. 1971 Subaqueous slope failures in Norwegian fjords. *Nor. Geotech. Inst. Bull.* **88**, 1–8.

Borrero, J. C. 2002 Re-analysis of field data provides better prediction: an example from Papua New Guinea. In *Proc. Int. Tsunami Symp., 7–10 August 2001, Seattle, WA*, pp. 297–305. National Oceanic and Atmospheric Administration.

Borrero, J. C., Dolan, J. F. & Synolakis, C. E. 2001 Tsunamis within the eastern Santa Barbara Channel. *Geophys. Res. Lett.* **28**, 643–646.

Brekhovskikh, L. M. & Lysanov, Yu. P. 1991 *Fundamentals of ocean acoustics.* Springer.

Davies, H. 1998 *The Sissano Tsunami.* Port Moresby: University of Papua New Guinea.

Doxsee, W. W. 1948 The Grand Banks earthquake of November 18, 1929. *Dom. Obs. Pub. Ottawa* **7**, 323–325.

Dziewonski, A. M., Ekström, G. & Maternovskaya, N. 1999 Centroid-moment tensor solutions for July–September 1998. *Phys. Earth Planet. Inter.* **114**, 99–107.

Eissler, H. K. & Kanamori, H. 1987 A single-force model for the 1975 Kalapana, Hawaii earthquake. *J. Geophys. Res.* **92**, 4827–4836.

Fukao, Y. 1979 Tsunami earthquake and subduction processes near deep sea trenches. *J. Geophys. Res.* **84**, 2303–2314.

Geist, E. L. 2000 Origin of the 17 July 1998 Papua New Guinea tsunami: earthquake or landslide? *Seism. Res. Lett.* **71**, 344–351.

Grilli, S. T. & Watts, P. 1999 Modeling of waves generated by a moving submerged body. Applications to underwater landslides. *Engng Analysis Bound. Elem.* **23**, 645–656.

Gutenberg, B. 1939 Tsunamis and earthquakes. *Bull. Seism. Soc. Am.* **29**, 517–526.

Hasegawa, H. S. & Kanamori, H. 1987 Source mechanism of the magnitude 7.2 Grand Banks earthquake of November 18, 1929: double-couple or submarine landslide? *Bull. Seism. Soc. Am.* **77**, 1984–2004.

Heinrich, P. 1992 Non-linear water waves generated by submarine and aerial landslides. *J. Wtrwy Port Coast. Ocean Engng* **118**, 249–266.

Heinrich, P., Piatanesi, A., Okal, E. A. & Hébert, H. 2000 Near-field modeling of the July 17, 1998 tsunami in Papua New Guinea. *Geophys. Res. Lett.* **27**, 3037–3040.

Hurukawa, N., Tsuji, Y. & Waluyo, B. 1999 A fault plane of the 1998 Papua New Guinea earthquake estimated from relocated aftershocks—combination of the International Data Center of CTBT, Meteorological and Geophysical Agency of Indonesia and temporal aftershock observation. *Eos* **80**, F751. (Abstract.)

Imamura, F. & Hashi, K. 2000 Re-examination of the tsunami source of the 1998 PNG earthquake tsunami. *Eos* **81**, WP143. (Abstract.)

Imamura, F., Gica, E., Takahashi, T. & Shuto, N. 1995 Numerical simulation of the 1992 Flores tsunami: interpretation of tsunami phenomena in northeastern Flores Island and damage at Babi Island. *Pure Appl. Geophys.* **144**, 555–568.

Jiang, L. & LeBlond, P. H. 1992 The coupling of a submarine slide and the surface wave which it generates. *J. Geophys. Res.* **97**, 12731–12744.

Jost, M. L. & Herrmann, R. B. 1989 A student guide to, a review of, moment tensors. *Seism. Res. Lett.* **60**, 37–57.

Joyner, W. B. & Boore, D. M. 1981 Peak horizontal acceleration and velocity from strong-motion records including records from the 1979 Imperial Valley, California earthquake. *Bull. Seism. Soc. Am.* **71**, 2011–2038.

Kanamori, H. 1970 The Alaska earthquake of 1964—radiation of long-period surface waves and source mechanism. *J. Geophys. Res.* **75**, 5029–5040.

Kanamori, H. 1972 Mechanisms of tsunami earthquakes. *Phys. Earth Planet. Inter.* **6**, 346–359.

Kanamori, H. 1985 Non-double-couple seismic source. In *Proc. 23rd Gen. Assemb. Int. Ass. Seism. Phys. Earth Inter., Tokyo*, p. 425. (Abstract.)

Kanamori, H. & Anderson, D. L. 1975 Amplitude of the Earth's free oscillations and long-period characteristics of the earthquake source. *J. Geophys. Res.* **80**, 1075–1078.

Kanamori, H. & Cipar, J. J. 1974 Focal process of the great Chilean earthquake, May 22, 1960. *Phys. Earth Planet. Inter.* **9**, 128–136.

Kanamori, H., Given, J. W. & Lay, T. 1984 Analysis of seismic waves excited by the Mount St Helens eruption of May 18, 1980. *J. Geophys. Res.* **89**, 1856–1866.

Kanoğlu, U. & Synolakis, C. E. 1998 Long wave runup on piecewise linear topographies. *J. Fluid Mech.* **374**, 1–28.

Kawata, Y., Benson, B. C., Borrero, J. C., Borrero, J. L., Davies, H. L., de Lang, W. P., Imamura, F., Letz, H., Nott, J. & Synolakis, C. E. 1999 The July 17, 1998, Papua New Guinea earthquake and tsunami. *Eos* **80**, 101.

Kikuchi, M., Yamanaka, Y., Abe, K., Morita, Y. & Watada, S. 1998 Source rupture process of the Papua New Guinea earthquake of July 17, 1998 inferred from teleseismic body waves. *Eos* **79**, F573. (Abstract.)

Kulikov, E. A., Rabinovich, A. B., Thomson, R. E. & Bornhold, B. D. 1996 The landslide tsunami of November 3, 1994, Skagway Harbor, Alaska. *J. Geophys. Res.* **101**, 6609–6615.

Lynett, P. & Liu, P. L.-F. 2001 Submarine landslide generated waves and run-up. In *Proc. NATO Adv. Res. Workshop, Istanbul, 23–26 May 2001.* (Abstract.)

Ma, K.-F., Satake, K. & Kanamori, H. 1991 The origin of the tsunami excited by the 1989 Loma Prieta earthquake: faulting or slumping? *Geophys. Res. Lett.* **18**, 637–640.

McCue, K. F. 1998 An AGSO perspective on PNG's tsunamigenic earthquake of 17 July 1998. *Aus. Geo. Int.* **9**, 1–2.

McSaveney, M. J., Goff, J. R., Darby, D. J., Goldsmith, P., Barnett, A., Elliott, S. & Nongkas, M. 2000 The 17 July 1998 tsunami, Papua New Guinea, evidence and initial interpretation. *Mar. Geol.* **170**, 81–92.

Mansinha, L. & Smylie, D. E. 1971 The displacement field of inclined faults. *Bull. Seism. Soc. Am.* **61**, 1433–1440.

Matsuyama, M., Walsh, J. P. & Yeh, H. 1999 The effect of bathymetry on tsunami characteristics at Sissano Lagoon, Papua New Guinea. *Geophys. Res. Lett.* **26**, 3513–3516.

Milne, J. 1898 *Earthquakes and other Earth movements.* London: Paul, Trench, Trübner & Co.

Montessus de Ballore, F. 1907 *La science séismologique.* Paris: A. Colin.

Murty, T. S. 1979 Submarine slide-generated water waves in Kitimat Inlet, British Columbia. *J. Geophys. Res.* **84**, 7777–7779.

Neuhauss, R. 1911 *Deutsch Neu-Guinea.* Berlin: Dietrich Reimer.

Newman, A. V. & Okal, E. A. 1998 Teleseismic estimates of radiated seismic energy: the E/M_0 discriminant for tsunami earthquakes. *J. Geophys. Res.* **103**, 26 885–26 898.

Okal, E. A. 1988 Seismic parameters controlling far-field tsunami amplitudes: a review. *Natural Hazards* **1**, 67–96.

Okal, E. A. 1992 Use of the mantle magnitude M_{m} for the reassessment of the seismic moment of historical earthquakes. I. Shallow events. *Pure Appl. Geophys.* **139**, 17–57.

Okal, E. A. 1999 The probable source of the 1998 Papua New Guinea tsunami as expressed in oceanic T waves. *Eos* **80**, F750. (Abstract.)

Okal, E. A. & Synolakis, C. E. 2001 Comment on 'Origin of the 17 July 1998 Papua New Guinea tsunami: earthquake or landslide?' by E. L. Geist. *Seism. Res. Lett.* **72**, 363–366.

Okal, E. A. & Talandier, J. 1989 M_{m}: a variable period mantle magnitude. *J. Geophys. Res.* **94**, 4169–4193.

Pelayo, A. M. & Wiens, D. A. 1992 Tsunami earthquakes: slow thrust-faulting events in the accretionary wedge. *J. Geophys. Res.* **97**, 15 321–15 337.

Pelinovsky, E. & Poplavsky, A. 1996 Simplified model of tsunami generation by submarine landslides. *Phys. Chem. Earth* **21**, 13–17.

Piper, D. J. W. & Aksu, A. E. 1987 The source and origin of the 1929 Grand Banks turbidity current inferred from sediment budgets. *Geo-Mar. Lett.* **7**, 177–182.

Plafker, G. 1965 Tectonic deformation associated with the 1964 Alaskan earthquake. *Science* **148**, 1675–1687.

Plafker, G. & Savage, J. C. 1970 Mechanism of the Chilean earthquakes of May 21 and 22, 1960. *Geol. Soc. Am. Bull.* **81**, 1001–1030.

Plafker, G., Kachadoorian, R., Eckel, E. B. & Mayo, L. R. 1969 Effects of the earthquake of March 27, 1964 on various communities. US Geol. Surv. Prof. Paper 542-G, US Geological Survey, Washington, DC.

Polet, J. & Kanamori, H. 2000 Shallow subduction zone earthquakes and their tsunamigenic potential. *Geophys. J. Int.* **142**, 684–702.

Prior, D. B. & Coleman, J. M. 1979 Submarine landslides: geometry and nomenclature. *Z. Geomorphol.* **23**, 415–426.

Satake, K. & Tanioka, Y. 1999 The July 1998 Papua New Guinea earthquake and tsunami: a generation model consistent with various observations. *Eos* **80**, F750–F751. (Abstract.)

Satake, K., Bourgeois, J., Abe, Ku., Abe, Ka., Tsuji, Y., Imamura, F., Iio, Y., Katao, H., Noguera, E. & Estrada, F. 1993 Tsunami field survey of the 1992 Nicaragua earthquake. *Eos* **74**, 145 and 156–157.

Schwab, W. C., Lee, H. J. & Twichell, D. C. (eds) 1993 Submarine landslides: selected studies in the US exclusive economic zone. *US Geol. Surv. Bull.* **B-2002**. Washington, DC: US Geological Survey.

Seed, H. B., Seed, R. B., Schlosser, F., Blondeau, F. & Juran, I. 1988 Report no. UCB/EERC-88/10. Earthquake Engineering Research Center, University of California, Berkeley, CA.

Smith, W. H. F. & Sandwell, D. T. 1997 Global seafloor topography from satellite altimetry and ship depth soundings. *Science* **277**, 1956–1962.

Sweet, S. 2000 Tectonics and slumping in the source region of the 1998 Papua New Guinea tsunami from seismic reflection images. MS thesis, University of California at Santa Cruz, CA.

Sweet, S. & Silver, E. A. 2002 Tectonics and slumping in the source region of the 1998 Papua New Guinea tsunami from seismic reflection images. *Appl. Geophys.* (In the press.)

Sweet, S., Silver, E. A., Davies, H., Matsumoto, T., Watts, P. & Synolakis, C. E. 1999 Seismic reflection images of the source region of the Papua New Guinea tsunami of July 17, 1998. *Eos* **80**, F750. (Abstract.)

Synolakis, C. E., Borrero, J. C., Plafker, G., Yalçiner, A., Greene, G. & Watts, P. 2000 Modeling the 1994 Skagway, Alaska tsunami. *Eos* **81**, F748. (Abstract.)

Tadepalli, S. & Synolakis, C. E. 1994 The run-up of N-waves on sloping beaches. *Proc. R. Soc. Lond.* A **445**, 99–112.

Tadepalli, S. & Synolakis, C. E. 1996 Model for the leading waves of tsunamis. *Phys. Rev. Lett.* **77**, 2141–2145.

Tanioka, Y. 1999 Analysis of the far-field tsunamis generated by the 1998 Papua New Guinea earthquake. *Geophys. Res. Lett.* **26**, 3393–3396.

Tanioka, Y. & Ruff, L. J. 1998 The 1998 Papua New Guinea earthquake, an outer rise event? *Eos* **79**, F572. (Abstract.)

Tappin, D. R. (and 18 others) 1999 Sediment slump likely caused 1998 Papua New Guinea tsunami. *Eos* **80**, 329, 334, 340.

Tappin, D. R., Watts, P., McMurtry, G. M., Lafoy, Y. & Matsumoto, T. 2001 The Sissano, Papua New Guinea Tsunami of July 1998—offshore evidence on the source mechanism. *Mar. Geol.* **175**, 1–23.

Titov, V. V. & Synolakis, C. E. 1998 Numerical modeling of tidal wave runup. *J. Wtrwy Port Coast. Ocean Engng* **124**, 157–171.

Tsuji, Y., Imamura, F., Matsutomi, H., Synolakis, C. E., Nanang, P. T., Jumadi, S., Harada, S., Han, S. S., Arai, K. & Cook, B. 1995 Field survey of the East Java earthquake and tsunami of June 3, 1994. *Pure Appl. Geophys.* **144**, 839–854.

Turner, A. K. & Schuster, R. L. (eds) 1996 Special Report 247. Transportation Research Board, Washington, DC.

Ward, S. N. 1980 Relationships of tsunami generation and an earthquake source. *J. Phys. Earth* **28**, 441–474.

Ward, S. N. 2001 Landslide tsunami. *J. Geophys. Res.* **106**, 11 201–11 215.

Watts, P. 2000 Tsunami features of solid block underwater landslides. *J. Wtrwy Port Coast. Ocean Engng* **126**, 144–152.

Watts, P., Borrero, J. C., Tappin, D. R., Bardet, J.-P., Grilli, S. T. & Synolakis, C. E. 1999 Novel simulation technique employed on PNG event. In *Proc. 22nd Gen. Assemb. International Union of Geodesy and Geophysics, Birmingham, UK* JSS42. (Abstract.)

Wessel, P. & Smith, W. H. F. 1991 Free software helps map and display data. *Eos* **72**, 441, 445–446.

Wysession, M. E., Okal, E. A. & Miller, K. L. 1991 Intraplate seismicity of the Pacific Basin, 1913–1988. *Pure Appl. Geophys.* **135**, 261–359.

Yalçiner, A. C., Borrero, J. C., Kanoğlu, U., Watts, P., Synolakis, C. E. & Imamura, F. 1999 Field survey of the 1999 Izmit tsunami and modeling effort of new tsunami generation mechanism. *Eos* **80**, F751. (Abstract.)